Tuning wave propagation in soft phononic crystals via large deformation and multi-field coupling effect

Bin Wu, Weiqiu Chen

Department of Engineering Mechanics
Zhejiang University, Hangzhou, China
E-mail: chenwq@zju.edu.cn

Outline

- **Introduction**
- **Nonlinear axisymmetric deformations**
- **Actuation of the DE cylinder with periodic electrical boundary conditions**
- **Dispersion relations (incremental L waves)**
- **Numerical results**
- **Conclusions**

Band gaps

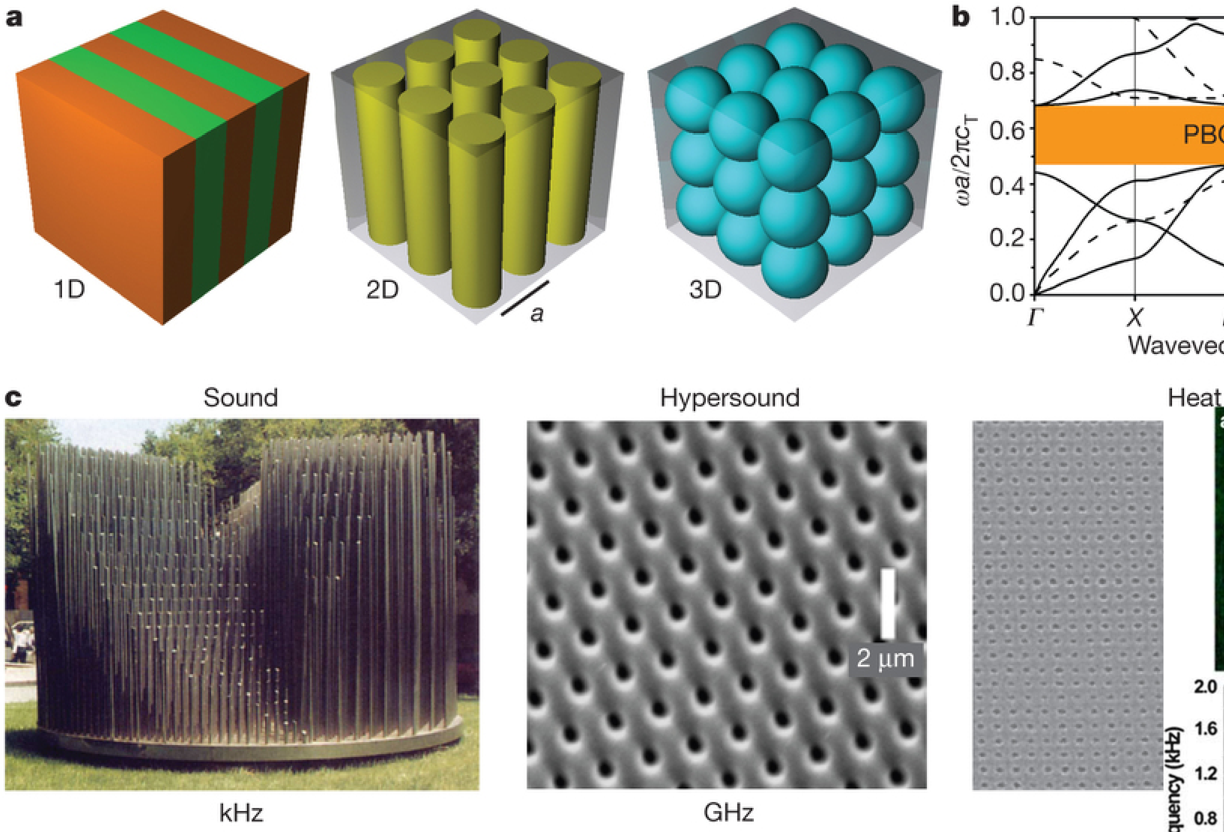

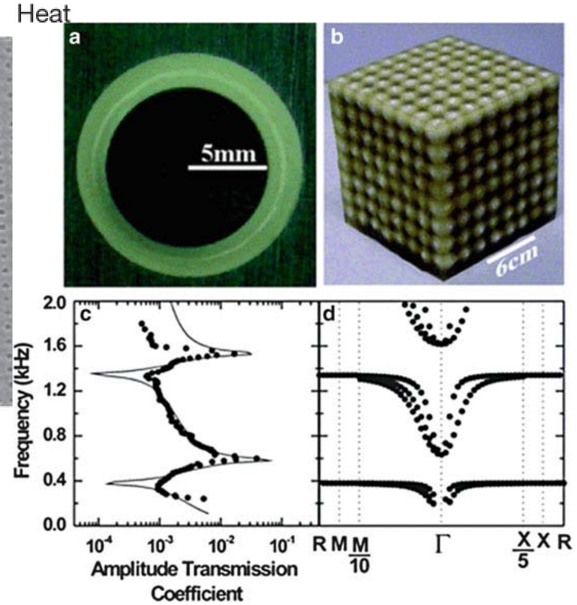

Periodic structures
(Maldovan, Nature, 2013)

Resonant units
(Liu & Sheng, Science, 2000)

Tuning band gaps

- Rotating the scatters (Goffaux and Vigneron, 2001)
- Making use of the effect of multifield coupling (Hou et al., 2004; Robillard et al., 2009; Yeh, 2007)
- Mechanical means: Prestress (Huang et al., 2014)
- Mechanical means: Large deformation (Bertoldi et al., 2008)

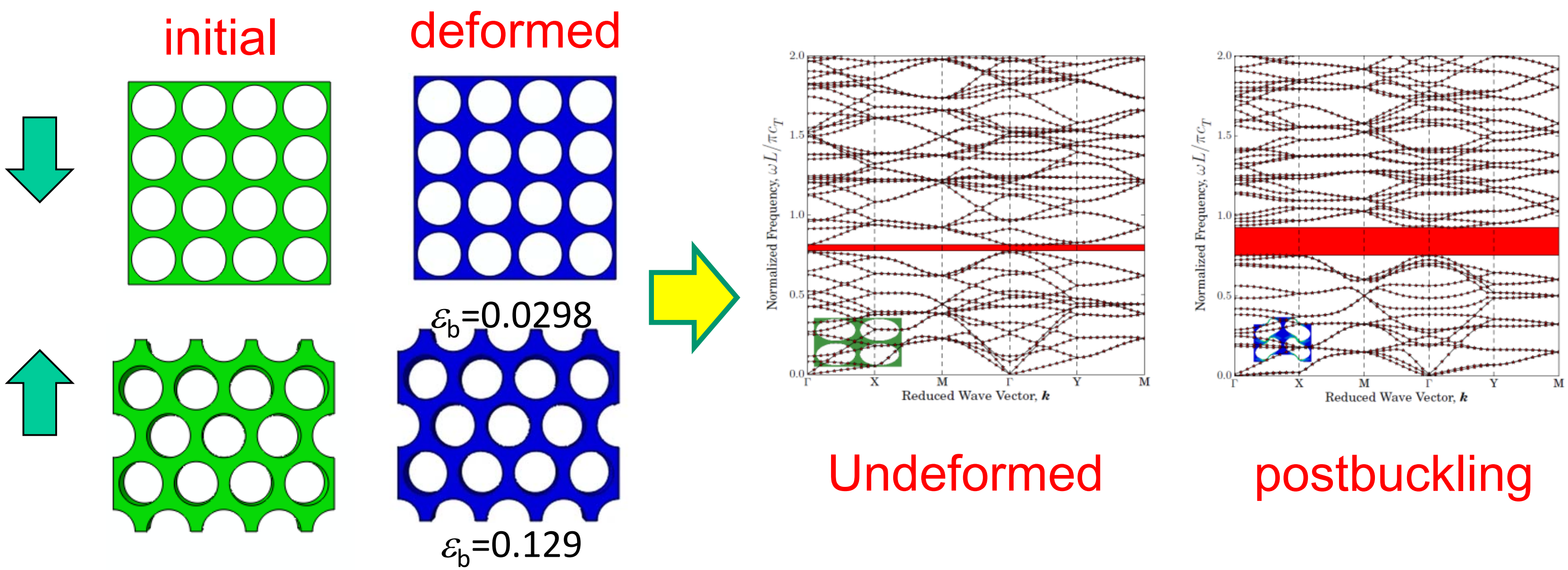

Some recent works

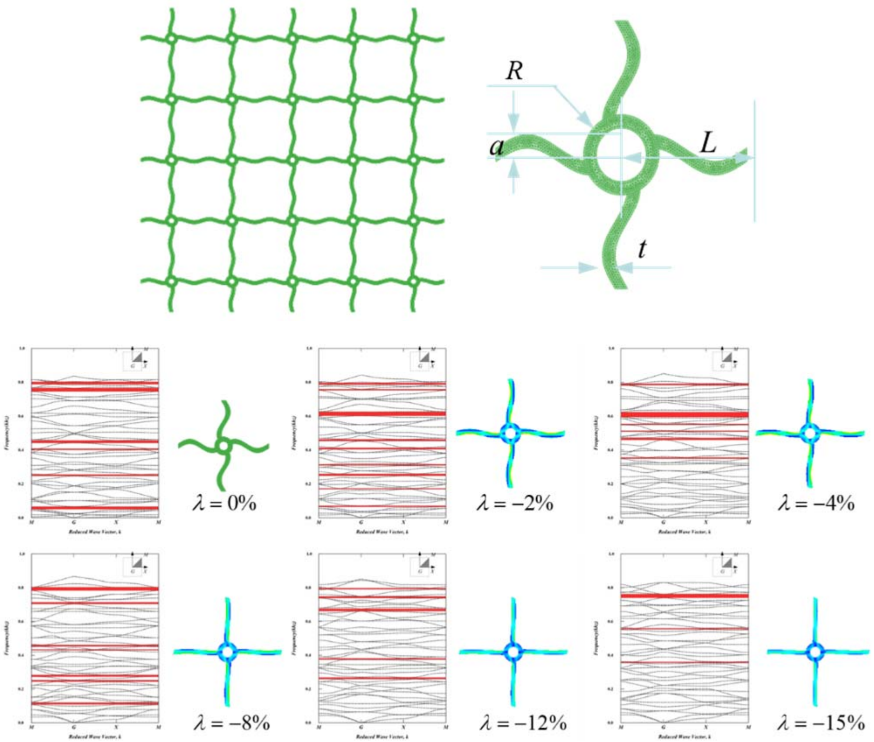

Tunable lattice phononics
Huang et al. AMSS (2018)

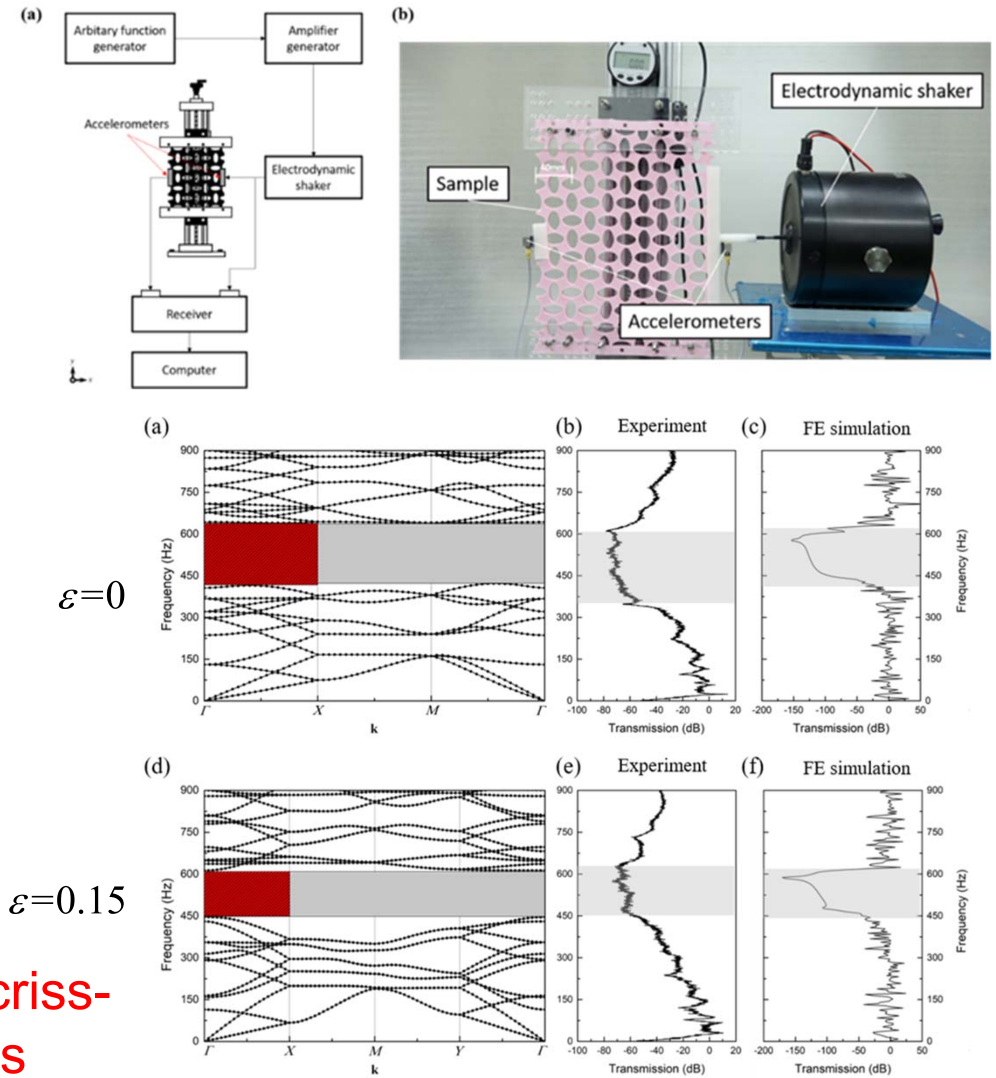

Tunable phononics with criss-crossed elliptical holes
Gao et al. In preparation

Some recent works

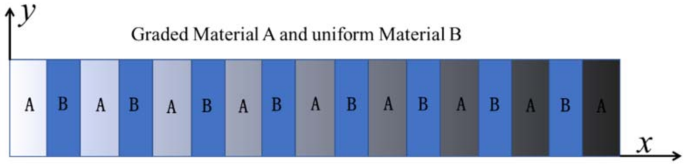

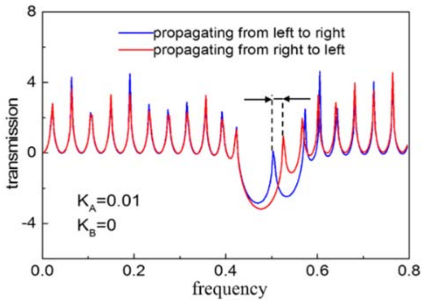

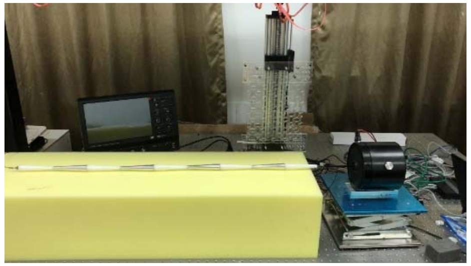

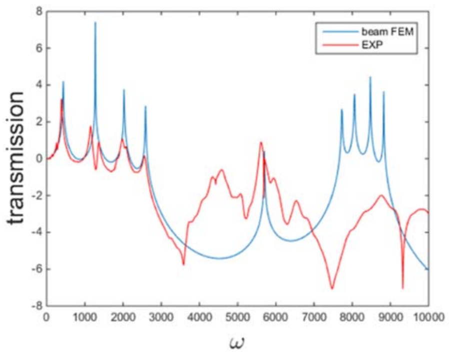

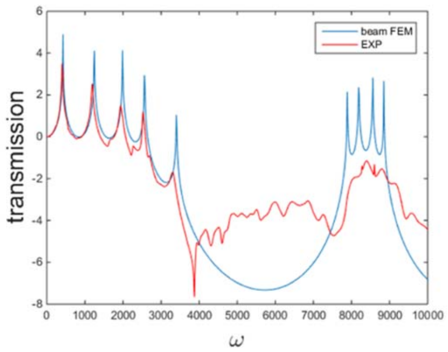

1D acoustic diode

Chen et al. JAM (2017)

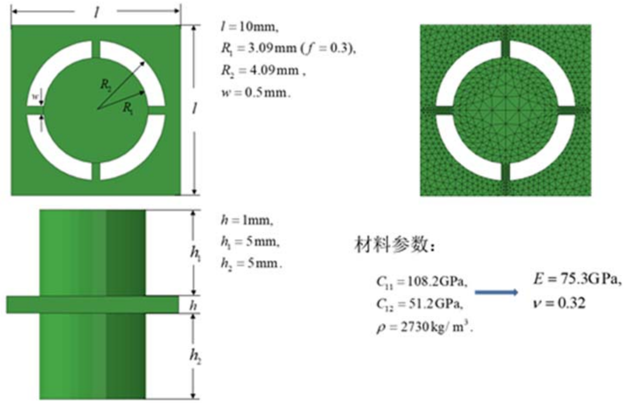

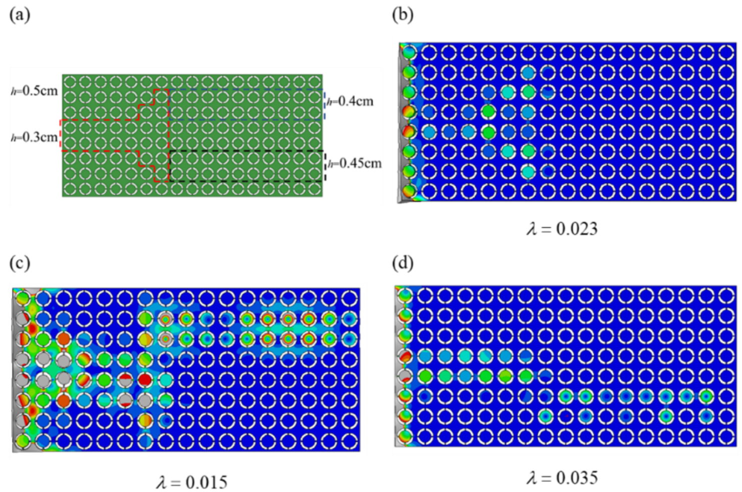

Tuning thorough small deformation

Huang et al. Submitted.

Outline

- Introduction
- **Nonlinear axisymmetric deformations**
- Actuation of the DE cylinder with periodic electrical boundary conditions
- Dispersion relations (incremental L waves)
- Numerical results
- Conclusions

Axisymmetric deformations

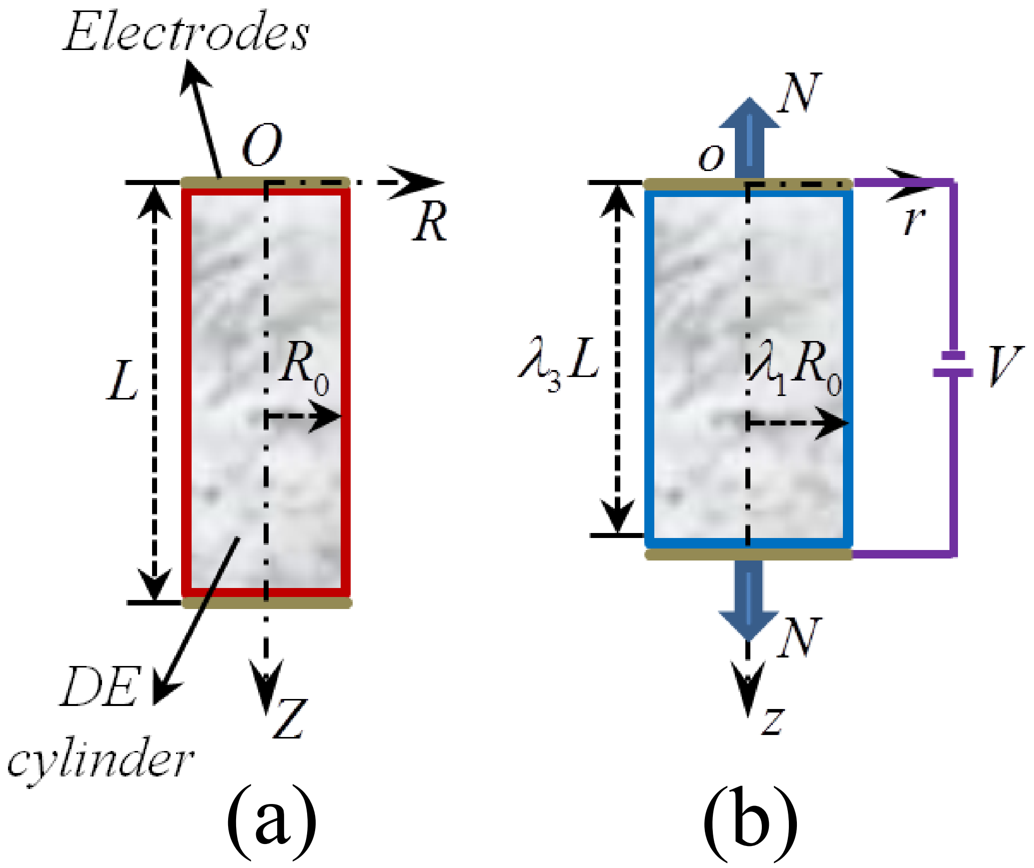

- Axisymmetric homogeneous deformations:

$$r = \lambda_1 R, \theta = \Theta, z = \lambda_3 Z,$$
$$\mathbf{F} = \mathrm{diag}[\lambda_1, \lambda_1, \lambda_3],$$
$$\boldsymbol{\sigma} = \mathrm{diag}[\sigma_{11}, \sigma_{22}, \sigma_{33}],$$
$$\mathbf{D} = [0, 0, D_3]^{\mathrm{T}}, \mathbf{E} = [0, 0, E_3]^{\mathrm{T}}$$

A soft DE cylinder with flexible electrodes:
(a) undeformed configuration; (b) activated configuration.

Axisymmetric deformations

➢ Ideal compressible dielectric elastomer (DE) model:

$$W = W_{\mathrm{elas}} + \frac{1}{2\varepsilon J}\lambda_3^2 D_{L3}^2, \quad J = \lambda_1\lambda_2\lambda_3, \quad \varepsilon = \varepsilon_0\varepsilon_r,$$

$$W_{\mathrm{elas}}^{nH} = \frac{\mu}{2}(I_1 - 3) - \mu \ln J + \frac{\Lambda}{2}(J-1)^2, \quad I_1 = \lambda_1^2 + \lambda_2^2 + \lambda_3^2,$$

$$W_{\mathrm{elas}}^{G} = -\frac{\mu J_m}{2}\ln\left(1 - \frac{I_1 - 3}{J_m}\right) - \mu \ln J + \left(\frac{\Lambda}{2} - \frac{\mu}{J_m}\right)(J-1)^2$$

μ --- initial shear modulus; Λ --- first Lame's parameter;

K --- bulk modulus; ε --- permittivity of the elastomer;

J_m --- Gent constant reflecting the limiting chain extensibility.

- Galich PI and Rudykh S (2016) Manipulating pressure and shear waves in dielectric elastomers via external electric stimuli. *Int. J. Solids Struct.* 91: 18-25.
- Galich PI, Fang NX, Boyce MC and Rudykh S (2017) Elastic wave propagation in finitely deformed layered materials. *J. Mech. Phys. Solids* 98: 390-410.

Axisymmetric deformations

- For neo-Hookean model:

$$\sigma_{11}=\sigma_{22}=\mu J^{-1}\left(\lambda_1^2-1\right)+\Lambda\left(J-1\right)-D_3^2/(2\varepsilon),$$

$$\sigma_{33}=\mu J^{-1}\left(\lambda_3^2-1\right)+\Lambda\left(J-1\right)+D_3^2/(2\varepsilon),\quad E_3=D_3/\varepsilon$$

- For Gent model:

$$\sigma_{11}=\sigma_{22}=\mu J^{-1}\left(\frac{J_m}{J_m-I_1+3}\lambda_1^2-1\right)+\left(\Lambda-\frac{2\mu}{J_m}\right)\left(J-1\right)-\frac{D_3^2}{2\varepsilon},$$

$$\sigma_{33}=\mu J^{-1}\left(\frac{J_m}{J_m-I_1+3}\lambda_3^2-1\right)+\left(\Lambda-\frac{2\mu}{J_m}\right)\left(J-1\right)+\frac{D_3^2}{2\varepsilon},E_3=\frac{D_3}{\varepsilon}$$

- Electric voltage applied to the electrodes:

$$V=-E_3 l=-\frac{D_3}{\varepsilon}\lambda_3 L,\quad \bar{V}^2=\bar{D}_3^2\lambda_3^2,\quad \bar{V}=\frac{V}{L}\sqrt{\frac{\varepsilon}{\mu}},\quad \bar{D}_3=\frac{D_3}{\sqrt{\mu\varepsilon}}$$

Axisymmetric deformations

- Traction boundary condition on the cylindrical surface and axial force condition:

$$\sigma_{11} = \sigma_{22} = 0, \quad \sigma_{33} = \frac{N}{\pi r_0^2} = \frac{N}{\pi \lambda_1^2 R_0^2}$$

- For neo-Hookean model:

$$\bar{\sigma}_{11} = \frac{\sigma_{11}}{\mu} = \bar{\sigma}_{22} = \frac{\sigma_{22}}{\mu} = \frac{1}{J}\left(\lambda_1^2 - 1\right) + \bar{\Lambda}\left(J - 1\right) - \frac{\bar{V}^2}{2\lambda_3^2} = 0,$$

$$\bar{\sigma}_{33} = \frac{\sigma_{33}}{\mu} = \frac{1}{J}\left(\lambda_3^2 - 1\right) + \bar{\Lambda}\left(J - 1\right) + \frac{\bar{V}^2}{2\lambda_3^2} = \frac{\bar{N}}{\lambda_1^2}, \quad \bar{\Lambda} = \frac{\Lambda}{\mu}, \quad \bar{N} = \frac{N}{\pi \mu R_0^2}$$

- For Gent model:

$$\bar{\sigma}_{11} = \bar{\sigma}_{22} = \frac{1}{J}\left(\frac{J_m}{J_m - I_1 + 3}\lambda_1^2 - 1\right) + \left(\bar{\Lambda} - \frac{2}{J_m}\right)\left(J - 1\right) - \frac{\bar{V}^2}{2\lambda_3^2} = 0,$$

$$\bar{\sigma}_{33} = \frac{1}{J}\left(\frac{J_m}{J_m - I_1 + 3}\lambda_3^2 - 1\right) + \left(\bar{\Lambda} - \frac{2}{J_m}\right)\left(J - 1\right) + \frac{\bar{V}^2}{2\lambda_3^2} = \frac{\bar{N}}{\lambda_1^2}$$

Outline

- Introduction
- Nonlinear axisymmetric deformations
- **Actuation of the DE cylinder with periodic electrical boundary conditions**
- Dispersion relations (incremental L waves)
- Numerical results
- Conclusions

Loading paths

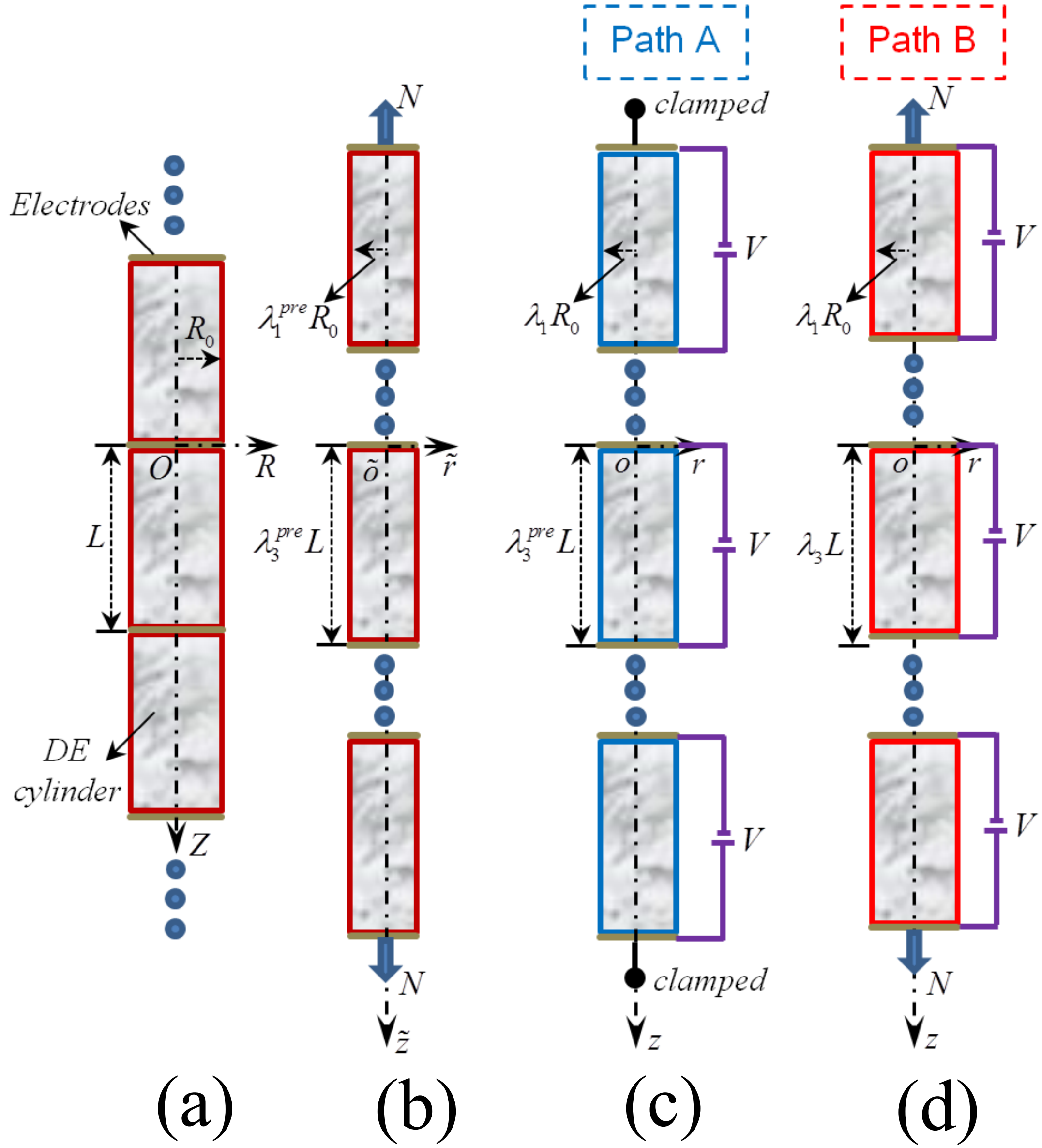

Geometry and actuation of the Infinitely long waveguide:

(a) undeformed configuration,

(b) pre-stretched configuration,

(c) path A configuration,

(d) path B configuration.

Path A (fixed axial pre-stretch)

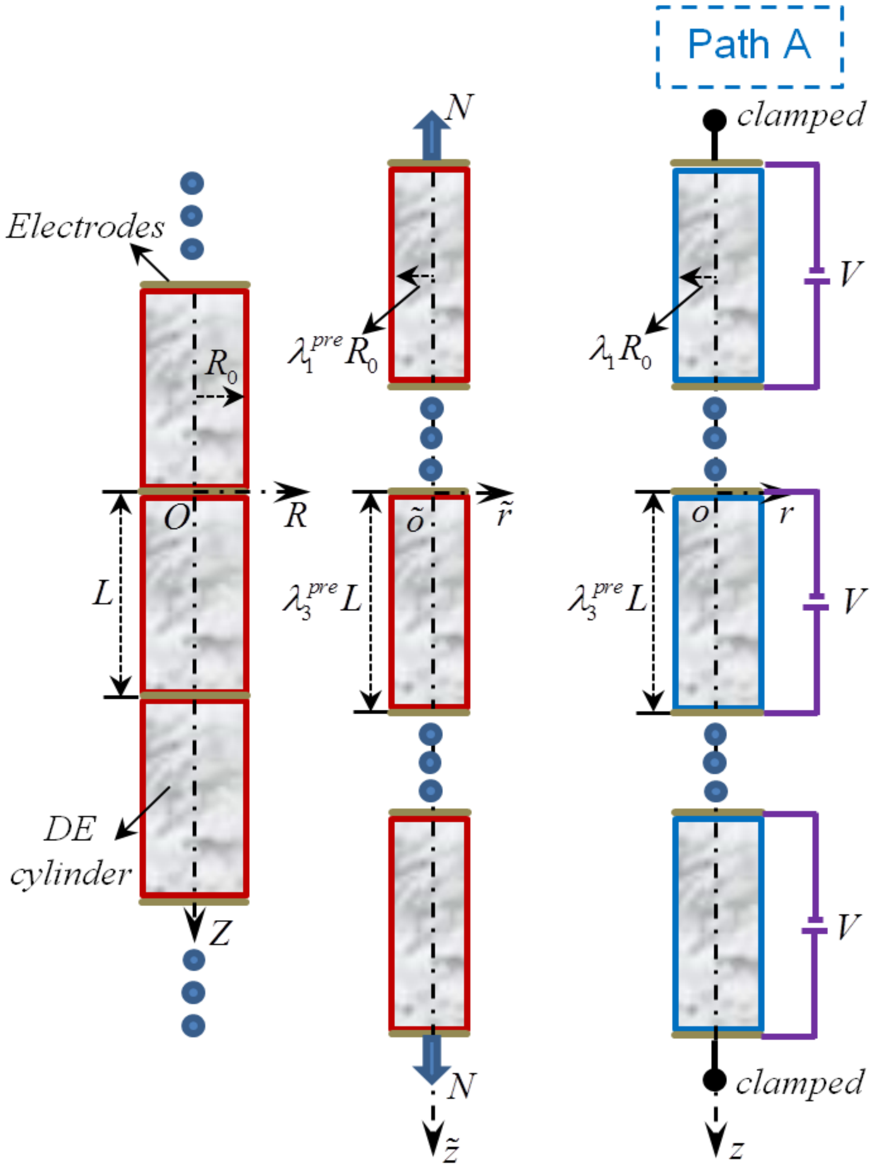

- First: Stretch with axial force but without voltage

$$\bar{V}=0,\quad \bar{\sigma}_{11}=\bar{\sigma}_{22}=0,\quad \bar{\sigma}_{33}=\bar{N}/\left(\lambda_1^{pre}\right)^2$$

λ_1^{pre}, λ_3^{pre} in terms of $\bar{N}$.

- Second: Keep the pre-stretch, and apply an electric voltage

$$\lambda_3^{pre}=\lambda_3,\quad \bar{\sigma}_{11}=\bar{\sigma}_{22}=0$$

λ_1, λ_3 in terms of $\bar{V}$ and λ_3^{pre}.

Path B (fixed axial force)

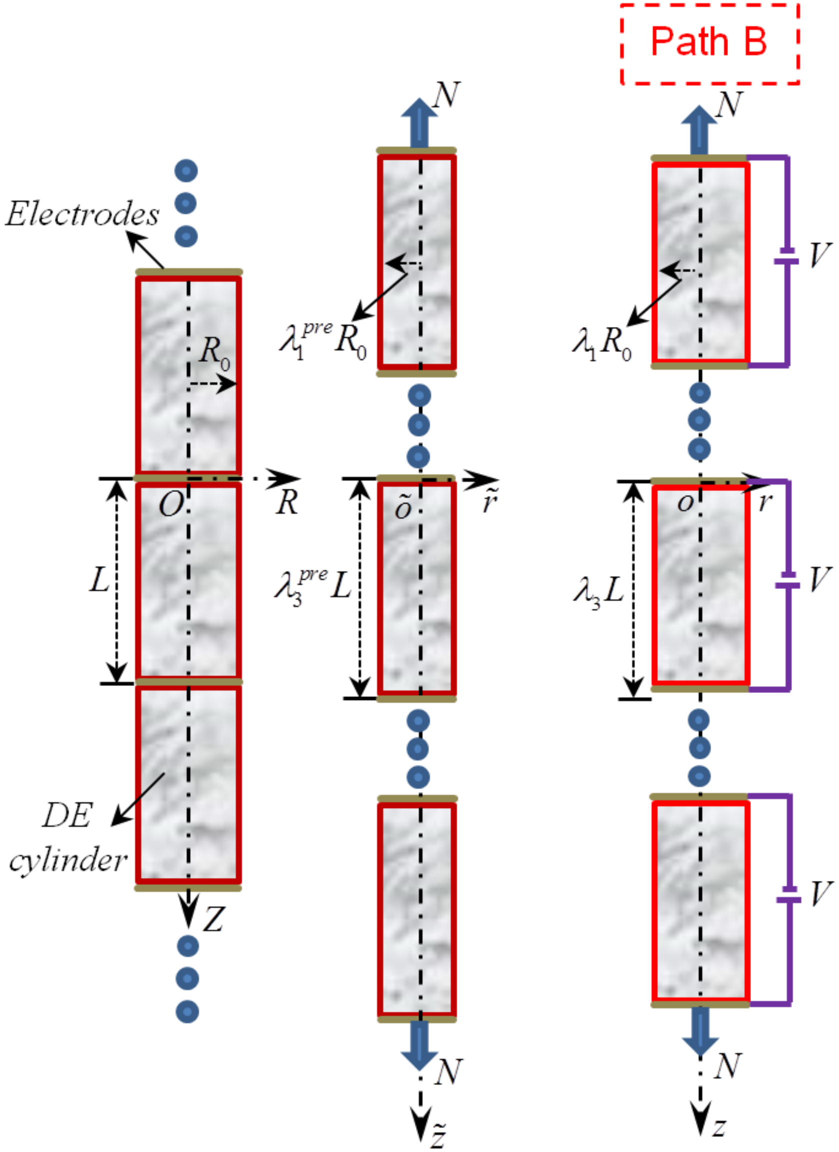

- First: Stretch with axial force but without voltage

$$\bar{V} = 0, \quad \bar{\sigma}_{11} = \bar{\sigma}_{22} = 0, \quad \bar{\sigma}_{33} = \bar{N} / \left(\lambda_1^{pre}\right)^2$$

$$\Downarrow$$

$\lambda_1^{pre}, \lambda_3^{pre}$ in terms of $\bar{N}$.

- Second: Keep the axial force and apply an electric voltage

$$\bar{\sigma}_{11} = \bar{\sigma}_{22} = 0, \quad \bar{\sigma}_{33} = \bar{N} / \lambda_1^2$$

$$\Downarrow$$

λ_1, λ_3 in terms of $\bar{V}$ and $\bar{N}$.

Outline

- Introduction
- Nonlinear axisymmetric deformations
- Actuation of the DE cylinder with periodic electrical boundary conditions
- **Dispersion relations (incremental L waves)**
- Numerical results
- Conclusions

1D Incremental equations

- Using the perturbation method, the linearized incremental constitutive equations in Lagrangian description:

$$\dot{S}_{11} = \mathcal{A}_{11}\dot{\lambda}_1 + \mathcal{A}_{12}\dot{\lambda}_2 + \mathcal{A}_{13}\dot{\lambda}_3 + \mathcal{B}_1\dot{D}_{L3}, \quad \dot{S}_{22} = \mathcal{A}_{12}\dot{\lambda}_1 + \mathcal{A}_{22}\dot{\lambda}_2 + \mathcal{A}_{23}\dot{\lambda}_3 + \mathcal{B}_2\dot{D}_{L3},$$

$$\dot{S}_{33} = \mathcal{A}_{13}\dot{\lambda}_1 + \mathcal{A}_{23}\dot{\lambda}_2 + \mathcal{A}_{33}\dot{\lambda}_3 + \mathcal{B}_3\dot{D}_{L3}, \quad \dot{E}_{L3} = \mathcal{B}_1\dot{\lambda}_1 + \mathcal{B}_2\dot{\lambda}_2 + \mathcal{B}_3\dot{\lambda}_3 + \mathcal{C}\dot{D}_{L3},$$

$$\mathcal{A}_{ij} = \mathcal{A}_{ji} = \frac{\partial^2 W}{\partial\lambda_i\partial\lambda_j}, \quad \mathcal{B}_j = \frac{\partial^2 W}{\partial\lambda_j\partial D_{L3}}, \quad \mathcal{C} = \frac{\partial^2 W}{\partial D_{L3}^2}$$

Stress relaxation condition: $\dot{S}_{11} = \dot{S}_{22} = 0$

- 1D incremental constitutive equations in Lagrangian description:

$$\dot{S}_{33} = \mathcal{A}^e\dot{\lambda}_3 + \mathcal{B}^e\dot{D}_{L3}, \quad \dot{E}_{L3} = \mathcal{B}^e\dot{\lambda}_3 + \mathcal{C}^e\dot{D}_{L3},$$

$$\mathcal{A}^e = \mathcal{A}_{33} - \mathcal{A}_{13}\mathcal{P}_{11} - \mathcal{A}_{23}\mathcal{P}_{21}, \quad \mathcal{B}^e = \mathcal{B}_3 - \mathcal{A}_{13}\mathcal{P}_{12} - \mathcal{A}_{23}\mathcal{P}_{22},$$

$$\mathcal{C}^e = \mathcal{C} - \mathcal{B}_1\mathcal{P}_{12} - \mathcal{B}_2\mathcal{P}_{22}, \quad \boldsymbol{\mathcal{P}} = \begin{bmatrix} \mathcal{A}_{11} & \mathcal{A}_{12} \\ \mathcal{A}_{12} & \mathcal{A}_{22} \end{bmatrix}^{-1} \begin{bmatrix} \mathcal{A}_{13} & \mathcal{B}_1 \\ \mathcal{A}_{23} & \mathcal{B}_2 \end{bmatrix}$$

1D Incremental equations

- Utilizing push-forward operation, 1D incremental constitutive equations in Eulerian description:

$$\dot{S}_{033} = J^{-1}\lambda_3\dot{S}_{33} = \mathcal{A}_0 e + \mathcal{B}_0\dot{D}_{L03}, \quad \dot{E}_{L03} = \lambda_3^{-1}\dot{E}_{L3} = \mathcal{B}_0 e + \mathcal{C}_0\dot{D}_{L03},$$

$$e = \dot{\lambda}_3/\lambda_3, \quad \dot{D}_{L03} = J^{-1}\lambda_3\dot{D}_{L3}, \quad \mathcal{A}_0 = J^{-1}\lambda_3^2\mathcal{A}^e, \quad \mathcal{B}_0 = \mathcal{B}^e, \quad \mathcal{C}_0 = J\lambda_3^{-2}\mathcal{C}^e$$

- 1D incremental governing equations:

$$\mathrm{div}\dot{\mathbf{S}}_0 = \rho\mathbf{u}_{,tt}, \quad \dot{S}_{033,3} = \rho w_{,tt},$$

$$\mathrm{div}\dot{\mathbf{D}}_{L0} = 0, \quad \dot{D}_{L03,3} = 0, \quad \dot{D}_{L03} = \text{constant}$$

- 1D equation of motion governing the time-harmonic incremental L waves:

$$\frac{d^2w}{dz'^2} + \varpi^2\kappa^2 w = 0, \quad z' = \frac{z}{l}, \quad \kappa^2 = \frac{\bar{\rho}}{\bar{\mathcal{A}}_0}, \quad \bar{\mathcal{A}}_0 = \frac{\mathcal{A}_0}{\mu},$$

$$\bar{\rho} = \rho/\rho_0, \quad \varpi^2 = \lambda_3^2\Omega^2, \quad \Omega^2 = \omega^2\rho_0 L^2/\mu$$

Dispersion relations

- Incremental displacement and stress:

$$w(z') = M_+ e^{i\varpi\kappa z'} + M_- e^{-i\varpi\kappa z'},$$

$$\dot{S}_{033}(z') = i\varpi\kappa\mathcal{A}_0\left(M_+ e^{i\varpi\kappa z'} - M_- e^{-i\varpi\kappa z'}\right)/l + \mathcal{B}_0\dot{D}_{L03}$$

- Bloch-Floquet relation at the interfaces:

$$w(1) = w(0)\exp(iq),$$

$$\dot{S}_{033}(1) = \dot{S}_{033}(0)\exp(iq)$$

q------- Bloch wavenumber

- The voltage applied to the cell is kept invariant:

$$\dot{V} = -\int_0^l \dot{E}_{L03}dz = 0 \Longrightarrow l\dot{D}_{L03} = \mathcal{B}_0\left[w(0) - w(1)\right]/\mathcal{C}_0$$

- Dispersion relations of incremental L waves:

$$\boxed{s^2\left[1 - \alpha\frac{\sin(\kappa\varpi)}{\kappa\varpi}\right] - 2s\left[\cos(\kappa\varpi) - \alpha\frac{\sin(\kappa\varpi)}{\kappa\varpi}\right] + 1 - \alpha\frac{\sin(\kappa\varpi)}{\kappa\varpi} = 0}$$

Dispersion relations

- Dispersion relations corresponding to pass band:

$$\cos q = \left[\cos(\kappa\varpi) - \alpha\frac{\sin(\kappa\varpi)}{\kappa\varpi}\right] / \left[1 - \alpha\frac{\sin(\kappa\varpi)}{\kappa\varpi}\right], \quad \alpha = \frac{\bar{\mathcal{B}}_0^2}{\bar{\mathcal{A}}_0 \bar{\mathcal{C}}_0}$$

- The frequency limits of the band gaps at the border of Brillouin zone:

$$\kappa\varpi = (2m+1)\pi,$$

$$\tan(\kappa\varpi/2) = \kappa\varpi/(2\alpha) \quad \Longrightarrow \quad \boxed{\text{Stability Condition} \quad \alpha < 1}$$

- The frequency limits at the center of Brillouin zone:

$$\kappa\varpi = 2m\pi$$

- In the long wave limit, the effective wave velocity:

$$V_{eff}^2 = (1-\alpha) J \bar{\mathcal{A}}_0 c_T^2, \quad c_T^2 = \frac{\mu}{\rho_0} \quad \Longrightarrow \quad \alpha < 1$$

Outline

- Introduction
- Nonlinear axisymmetric deformations
- Actuation of the DE cylinder with periodic electrical boundary conditions
- Dispersion relations (incremental L waves)
- **Numerical results**
- Conclusions

Neo-Hookean model

- Effective material parameters:

$$\bar{\mathcal{C}} = \lambda_3^2 / J, \quad \bar{\mathcal{B}}_1 = \bar{\mathcal{B}}_2 = -\lambda_3 \bar{D}_3 / \lambda_1, \quad \bar{\mathcal{B}}_3 = \bar{D}_3,$$

$$\bar{\mathcal{A}}_{11} = \bar{\mathcal{A}}_{22} = 1 + \left(1 + J^2 \bar{\Lambda} + J \bar{D}_3^2\right) / \lambda_1^2, \bar{\mathcal{A}}_{12} = \bar{\Lambda}\left(2J - 1\right)\lambda_3 + \lambda_3 \bar{D}_3^2 / 2,$$

$$\bar{\mathcal{A}}_{13} = \bar{\mathcal{A}}_{23} = \bar{\Lambda}\left(2J - 1\right)\lambda_1 - \lambda_1 \bar{D}_3^2 / 2, \bar{\mathcal{A}}_{33} = 1 + \left(1 + J^2 \bar{\Lambda}\right) / \lambda_3^2$$

- Geometrical parameters and physical properties of Fluorosilicone 730:

$$\rho_0 = 1400\mathrm{kg/m^3}, \quad \mu = 167.67\mathrm{kPa}, \quad \Lambda = 100\mu,$$

$$\varepsilon_0 = 8.85 \times 10^{-12}\mathrm{F/m}, \quad \varepsilon_r = 7.11,$$

$$E_{EB} = 372\mathrm{MV/m}, \quad L = 50\mathrm{mm}, \quad R_0 = 10\mathrm{mm}$$

- Wave frequency :

$$\Omega^2 = \rho_0 \omega^2 L^2 / \mu, \quad f = \omega / (2\pi)$$

□ Shmuel and Pernas-Salomon (2016) Manipulating motions of elastomer films by electrostatically-controlled aperiodicity. *Smart Mater. Struct.* **25**: 125012.

Neo-Hookean model

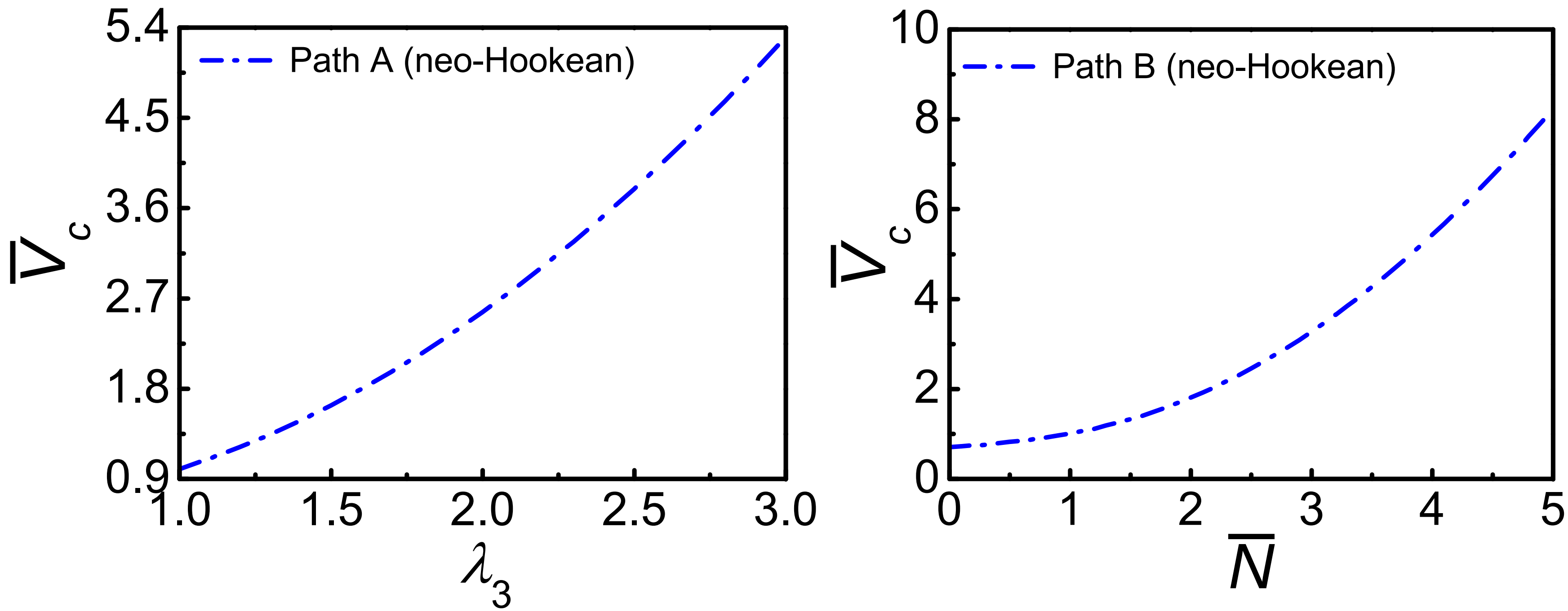

The critical voltages vs axial pre-stretch for Path A or axial force for Path B making wave velocity of the lowest branch vanish. ($\alpha = 1$)

Normalized electrical breakdown voltage

$$\bar{V}_{EB} = E_{EB}\lambda_3\sqrt{\varepsilon / \mu}$$

$>$

Critical voltage $\bar{V}_c$

Nonlinear response (path A)

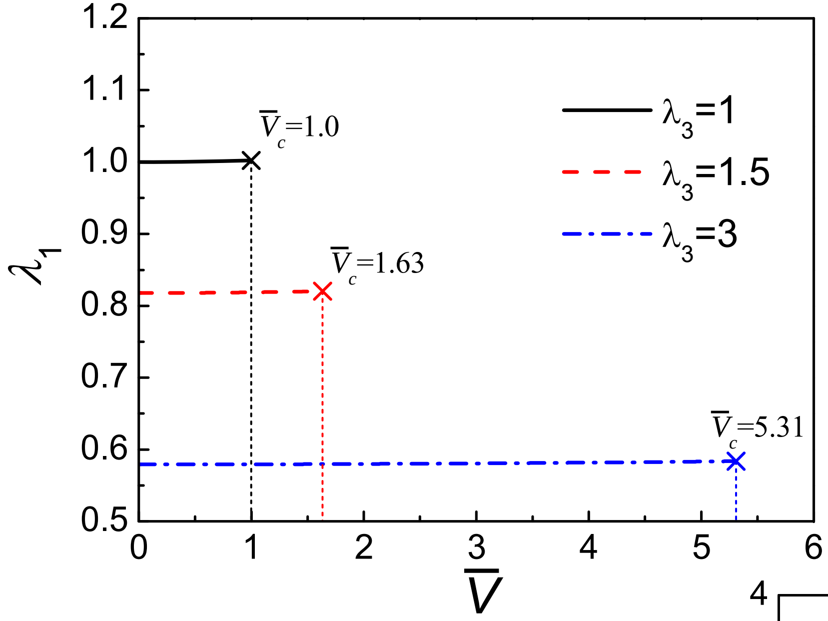

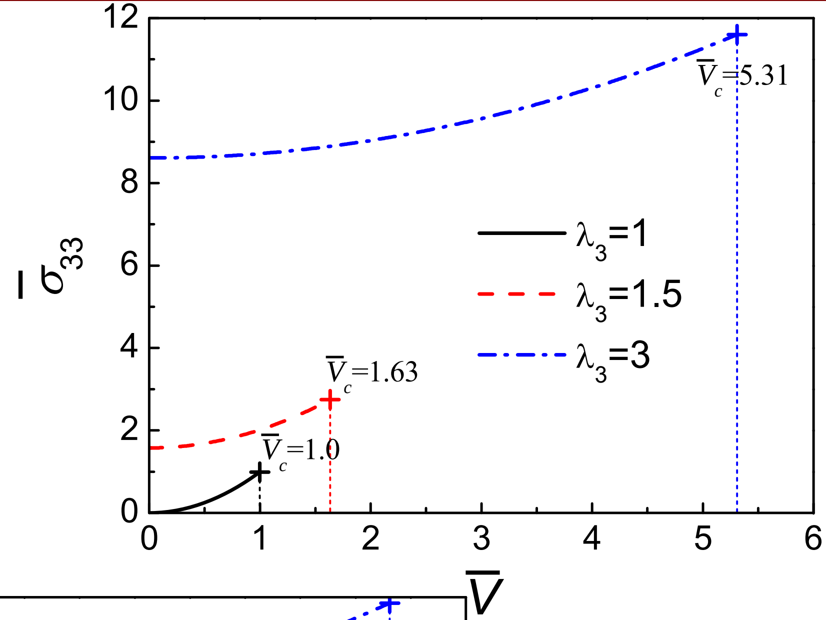

Nonlinear response to electric voltage at different pre-stretches for path A of neo-Hookean model.

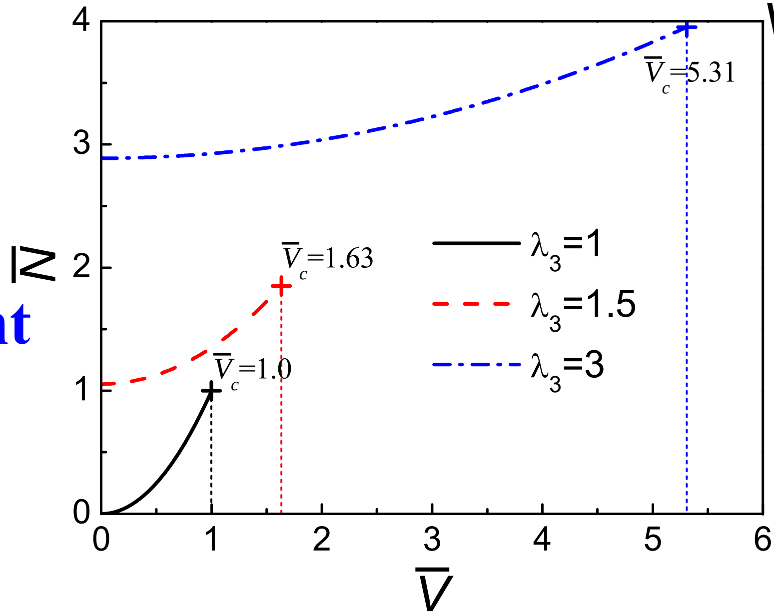

Dispersion curves (path A)

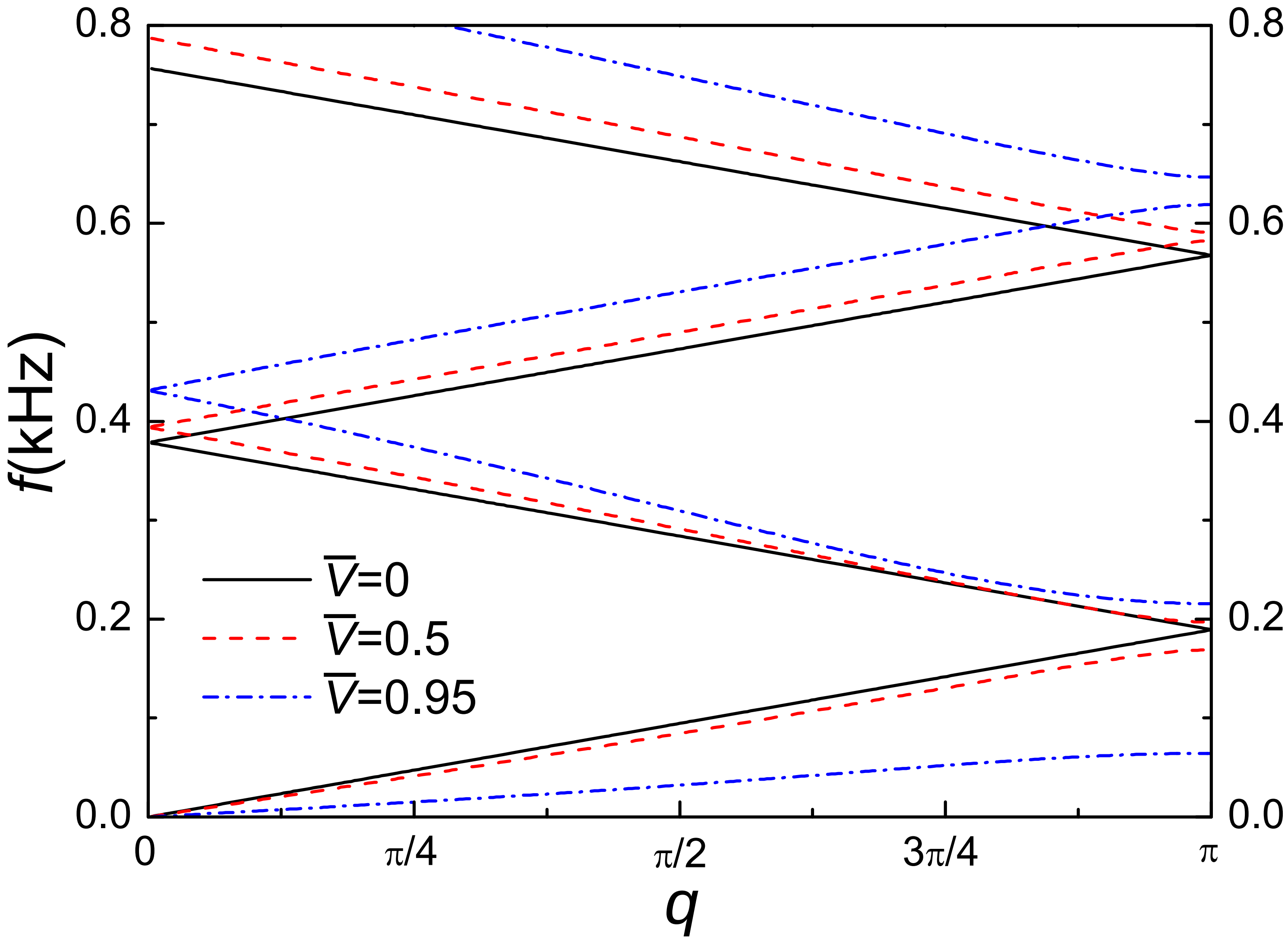

The first four dispersion curves at different voltages for $\lambda_3 = 1$.

Dispersion curves (path A)

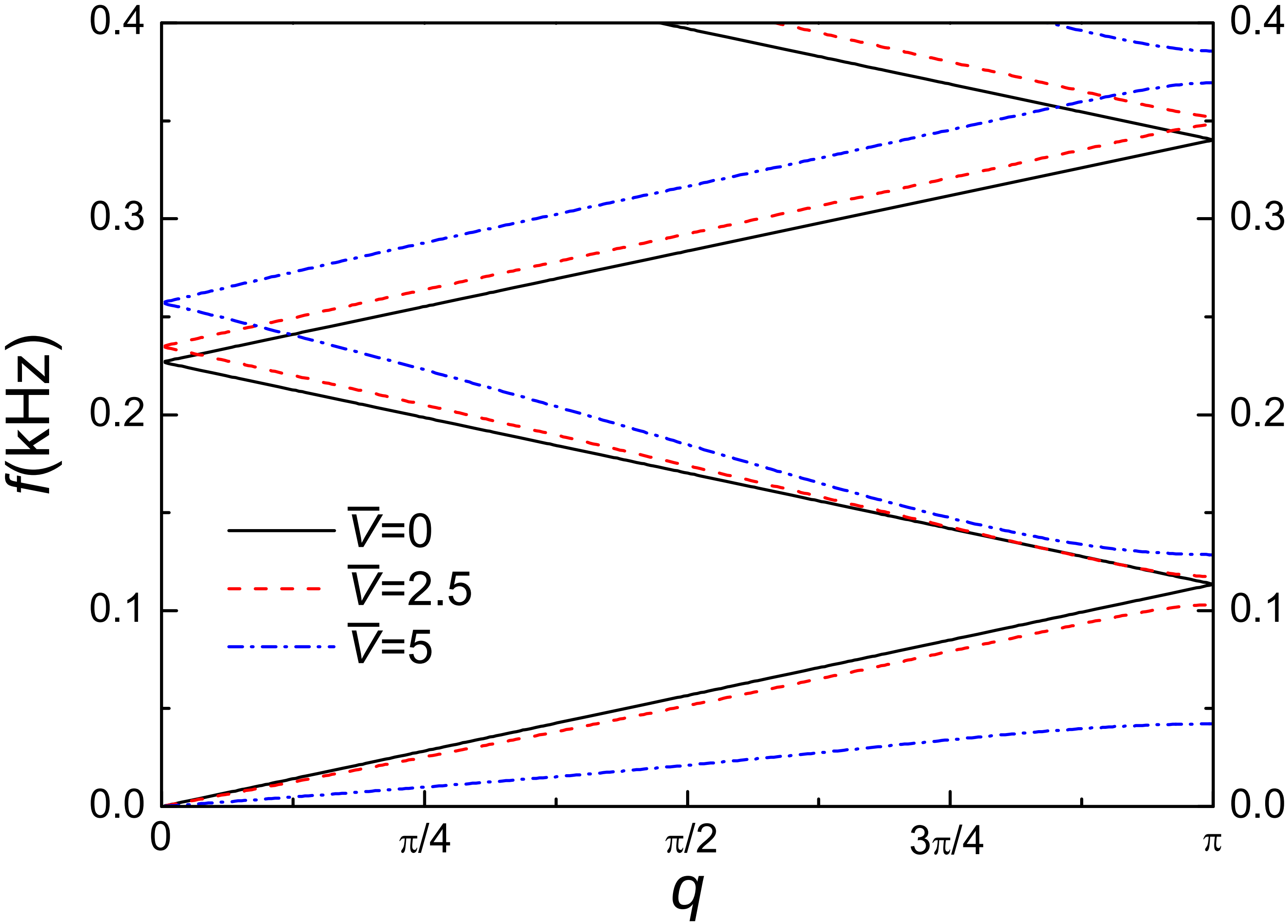

The first four dispersion curves at different voltages for $\lambda_3 = 3$.

Bragg band gaps (path A)

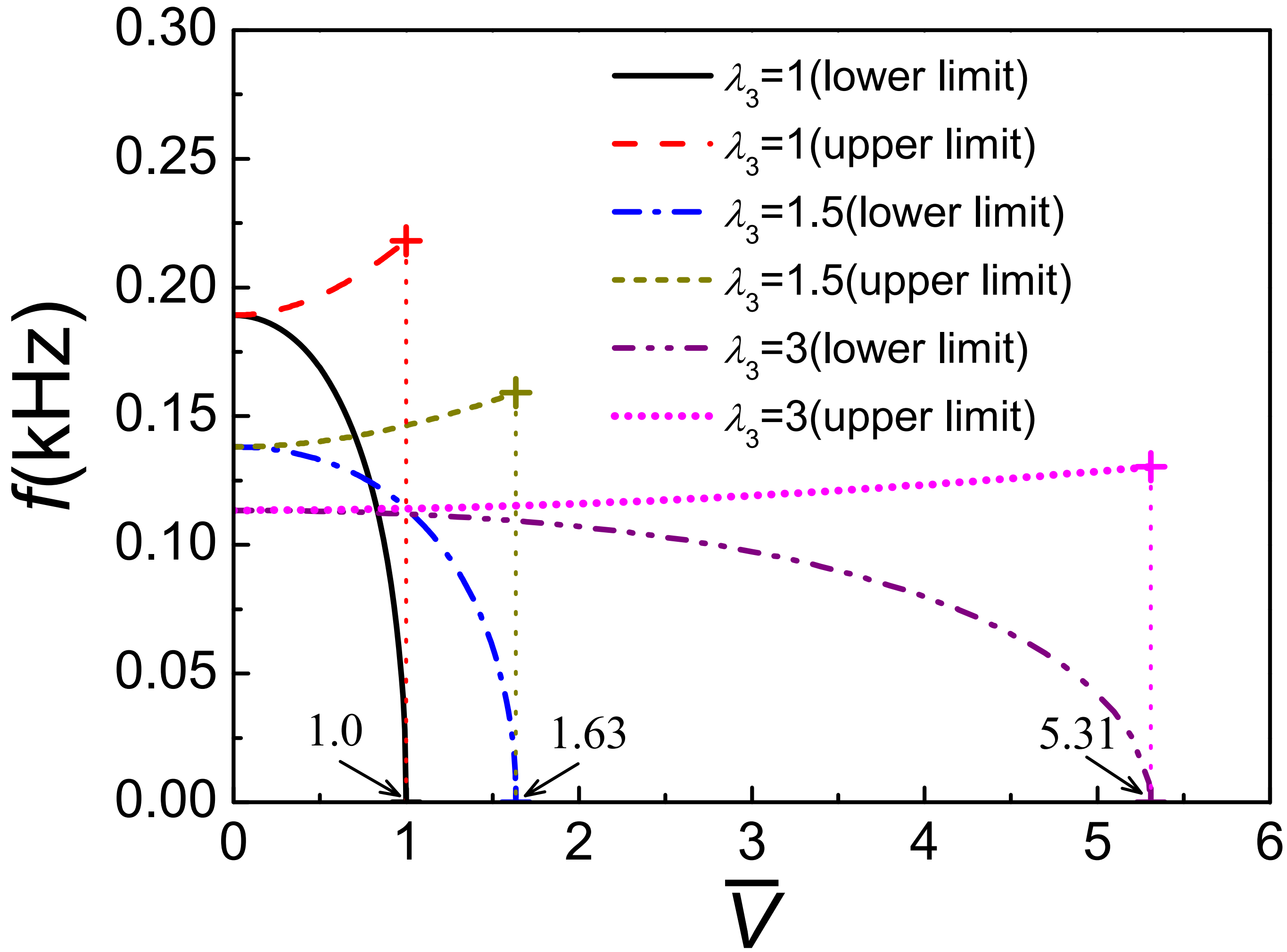

The variations of the lowest Bragg band gap with the electric voltage for different values of pre-stretches.

Bragg band gaps (path A)

Table 1. Tunable range of the 1st Bragg band gap for different axial pre-stretches.

Pre-stretch	Control range of normalized electric voltage ($\bar{V}$)	1st band gap central frequency (kHz)	Variation of 1st band gap normalized central frequency	1st band gap width (kHz)	Variation of 1st band gap normalized frequency width
$\lambda_3 = 1$	0-1.00	0.189-0.109	1-0.576	0-0.218	0-1.153
$\lambda_3 = 1.5$	0-1.63	0.138-0.080	1-0.580	0-0.159	0-1.152
$\lambda_3 = 3$	0-5.31	0.113-0.065	1-0.575	0-0.130	0-1.150

Geometry	Materials (matrix/inclusions)	Type of control	Control range or type of external impedance	Variation of 1st band gap normalized central frequency	Variation of 1st band gap normalized frequency width (%)
2D PC	Quartz/void	Temperature	0–50 °C	1–0.998	0.386–0.388
2D PC	Epoxy/electro-rheological material	DC electric field	0.5–3.5 kV m^{-1}	1–0.934	0.638–0.571
2D PC	Elastomer/void	Stress	92–95 kPa	1–1.044	0–0.0062
2D PC	Epoxy/Terfenol D	DC magnetic field	0–20 kOe	1–1.337	0–0.712
2D PC	PIN-PMN-PT/void	External impedance	0–+∞ nF	1–0.988	0.103–0.078
Beam with piezoelectric patches	Epoxy/Lead Zirconate Titanate (PZT)	External impedance	0—108 nF	1–1.714	0.286–1.714
Uniform rod	PZT	External impedance	0–+∞ nF	1–0.833	0–0.333

- Degraeve et al. (2014) Bragg band gaps tunability in an homogenoeous piezoelectric rod with periodic electrical boundary conditions. *J. Appl. Phys.* 115: 194508.

Long wave limit (path A)

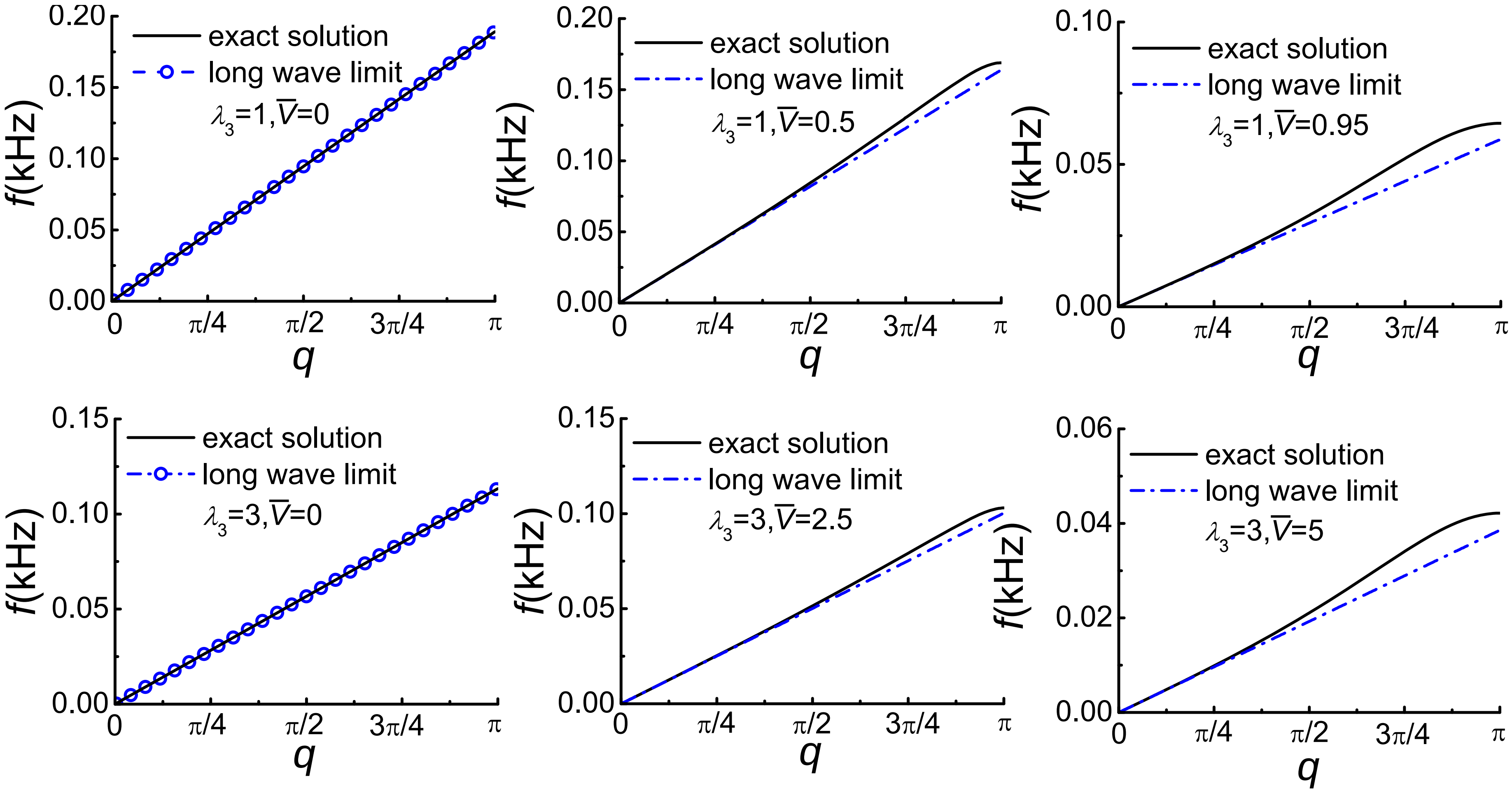

Comparison of the long wave limits with the exact dispersion relation for the incremental L waves at different axial pre-stretches and electric voltages.

Nonlinear response (path B)

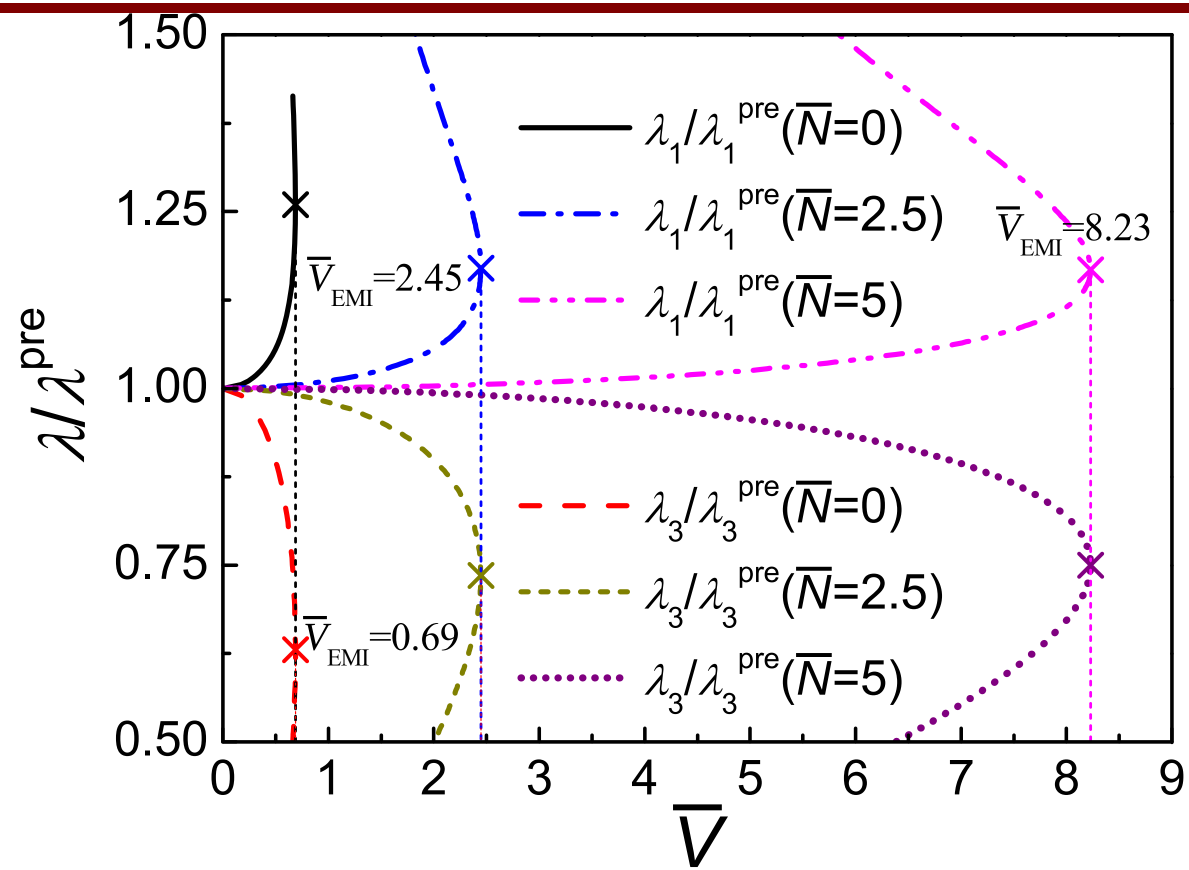

Nonlinear response to electric voltage at different axial force for path B of neo-Hookean model.

Electromechanical instability voltage $\overline{V}_{EMI}$ = Critical voltage $\overline{V}_c$

Dispersion curves (path B)

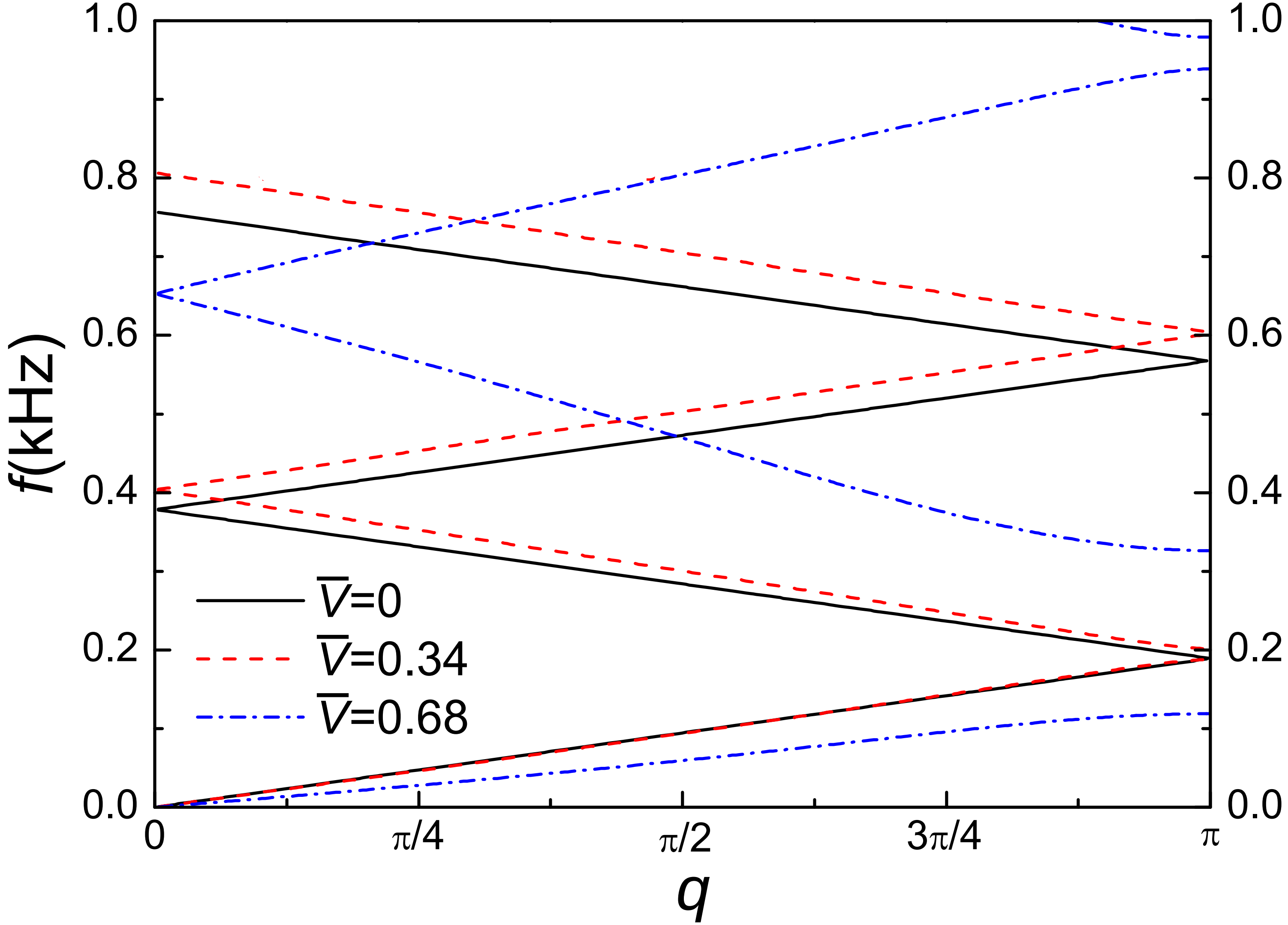

The first four dispersion curves at different voltages for $\bar{N}=0$ **.**

Nonlinear response (path B)

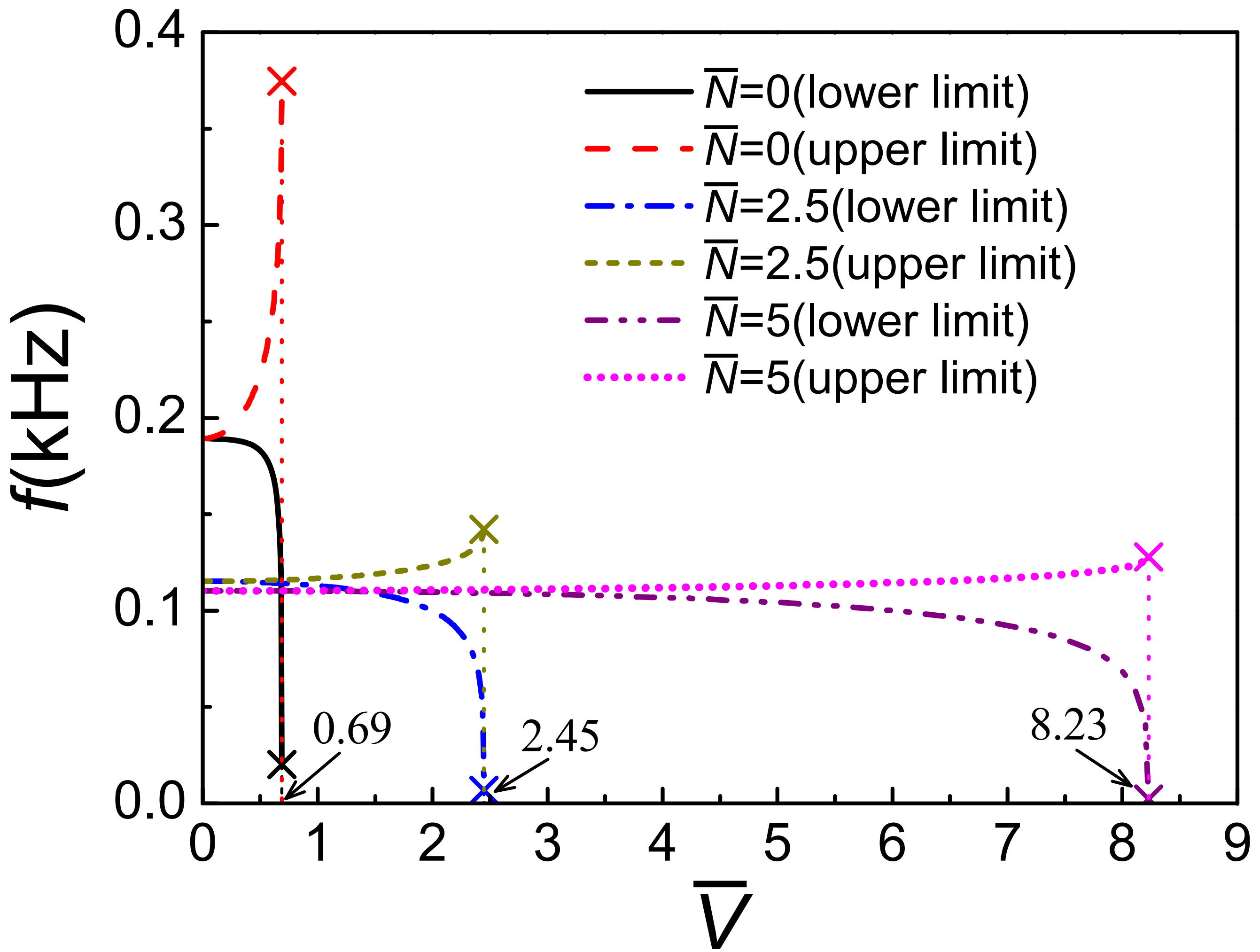

The variations of the lowest Bragg band gaps with the electric voltage for different values of axial forces.

Bragg band gaps (path B)

Table 1. Tunable range of the 1st Bragg band gap for different axial force.

Pre-stretch	Control range of normalized electric voltage ($\bar{V}$)	1st band gap central frequency (kHz)	Variation of 1st band gap normalized central frequency	1st band gap width (kHz)	Variation of 1st band gap normalized frequency width
$\bar{N}=0$	0-0.69	0.189-0.177	1-0.936	0-0.354	0-1.873
$\bar{N}=2.5$	0-2.45	0.115-0.074	1-0.646	0-0.135	0-1.174
$\bar{N}=5$	0-8.23	0.110-0.065	1-0.589	0-0.126	0-1.146

Geometry	Materials (matrix/inclusions)	Type of control	Control range or type of external impedance	Variation of 1st band gap normalized central frequency	Variation of 1st band gap normalized frequency width (%)
2D PC	Quartz/void	Temperature	0–50 °C	1–0.998	0.386–0.388
2D PC	Epoxy/electro-rheological material	DC electric field	0.5–3.5 kV m^{-1}	1–0.934	0.638–0.571
2D PC	Elastomer/void	Stress	92–95 kPa	1–1.044	0–0.0062
2D PC	Epoxy/Terfenol D	DC magnetic field	0–20 kOe	1–1.337	0–0.712
2D PC	PIN-PMN-PT/void	External impedance	0–+∞ nF	1–0.988	0.103–0.078
Beam with piezoelectric patches	Epoxy/Lead Zirconate Titanate (PZT)	External impedance	0—108 nF	1–1.714	0.286–1.714
Uniform rod	PZT	External impedance	0–+∞ nF	1–0.833	0–0.333

- Degraeve et al. (2014) Bragg band gaps tunability in an homogenoeous piezoelectric rod with periodic electrical boundary conditions. *J. Appl. Phys.* 115: 194508.

Gent model and snap-through transition

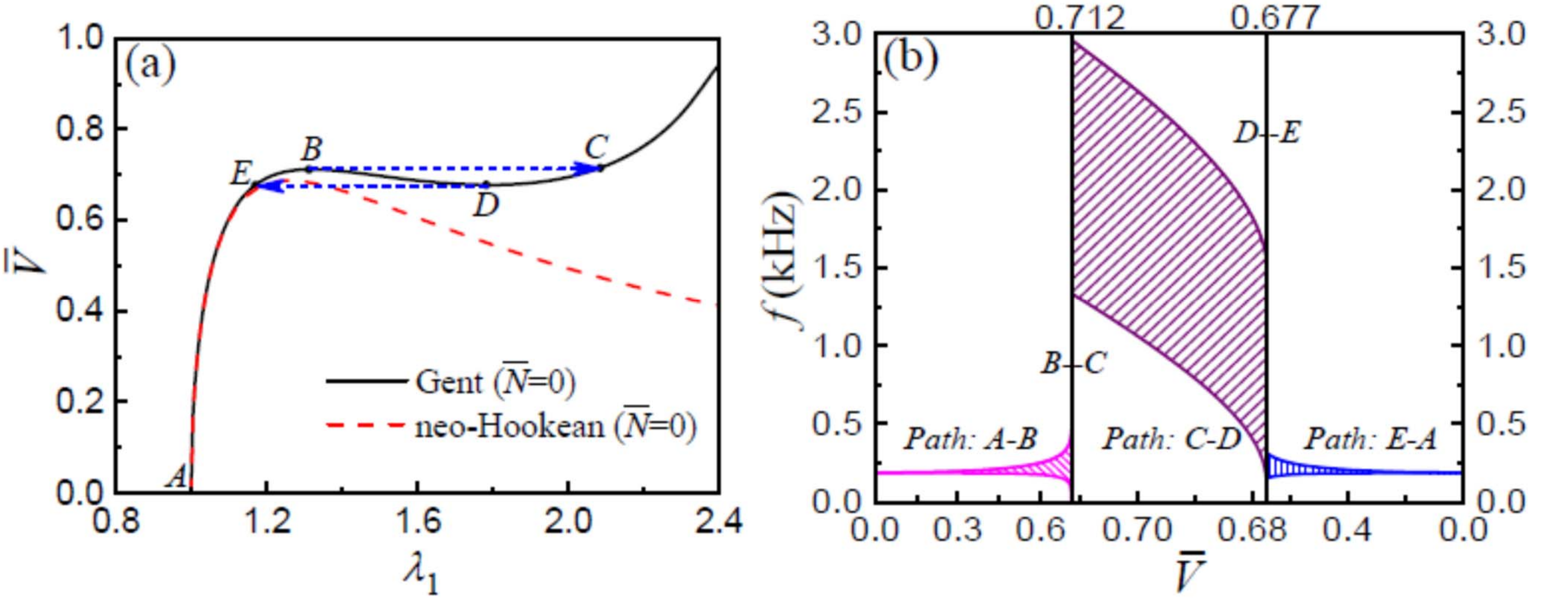

(a) Nonlinear response of the radial stretch to the dimensionless electric voltage in the axially free DE phononic cylinder for the neo-Hookean and Gent models. The snap-through transitions associated with the Gent model only are denoted by the blue dashed arrows. (b) The frequency limits of the first Bragg BG versus the dimensionless electric voltage in the axially free DE phononic cylinder for the Gent model.

Outline

- Introduction
- Nonlinear axisymmetric deformations
- Actuation of the DE cylinder with periodic electrical boundary conditions
- Dispersion relations (incremental L waves)
- Numerical results
- **Conclusions**

Conclusions

- ✓ Analytical dispersion relations for longitudinal waves in are obtained within the **Dorfmann-Ogden framework of electroelasticity** for 1D soft DE phononic crystal cylinders.
- ✓ Nonlinear response of two loading paths, i.e. fixed axial pre-stretch (Path A) and fixed axial force (Path B), are considered. The frequency limits of band gaps and the long wave limits are derived analytically.
- ✓ The nonlinear response and Bragg band gap is confined by the critical voltage. The applied voltage can largely widen the band gaps while the pre-stretch or axial force mainly change the position. The effective wave velocity at low frequency and long wavelength can be tuned by the pre-stretch and the applied voltage.
- ✓ **The increasing axial pre-stretch or axial force, while enhancing the stability of the 1D phononic crystal, weakens its working performance in terms of the tunable band gap width.**

Thanks for your attention!

The work was sponsored by the National Natural Science Foundation of China (Nos. 11532001 and 11621062).

Welcome to Hangzhou!

Welcome to Hangzhou!

12th International Congress on Thermal Stresses
June 1-5, 2019, Hangzhou, China

General Chair

Prof. Weiqiu Chen
Department of Engineering Mechanics
Zhejiang University, Hangzhou 310027, Zhejiang, China, phone: +86-571-87951866
Emails: chenwq@zju.edu.cn

Secretariat of TS 2019

Prof. Jizhou Song
Department of Engineering Mechanics
Zhejiang University, Hangzhou, China
Tel: +86-571-87952368
E-mail: jzsong@zju.edu.cn
ts2019zju@gmail.com

Co-Chairs

Prof. Richard B Hetnarski
Rochester Institute of Technology, USA
Prof. Naotake Noda
Shizuoka University, Japan

Web: http://ts2019.zju.edu.cn